JCTC Journal of Chemical Theory and Computation

Article

pubs.acs.org/JCTC

General-Order Many-Body Green's Function Method

So Hirata,*[,†] Matthew R. Hermes,[†] Jack Simons,[‡] and J. V. Ortiz[§]

[†]Department of Chemistry, University of Illinois at Urbana−Champaign, Urbana, Illinois 61801, United States

[‡]Department of Chemistry, University of Utah, Salt Lake City, Utah 84112, United States

[§]Department of Chemistry and Biochemistry, Auburn University, Auburn, Alabama 36849-5312, United States

ABSTRACT: Electron binding energies are evaluated as differences in total energy between the N- and $(N \pm 1)$-electron systems calculated by the nth-order Møller−Plesset perturbation (MPn) theory using the same set of orbitals. The MPn energies up to $n = 30$ are, in turn, obtained by the determinant-based method of Knowles et al. (*Chem. Phys. Lett.* **1985**, *113*, 8−12). The zeroth- through third-order electron binding energies thus determined agree with those obtained by solving the Dyson equation in the diagonal and frequency-independent approximations of the self-energy. However, as $n \to \infty$, they converge at the exact basis-set solutions from the Dyson equation with the exact self-energy, which is nondiagonal and frequency-dependent. This suggests that the MPn energy differences define an alternative diagrammatic expansion of Koopmans-like electron binding energies, which takes into account the perturbation corrections from the off-diagonal elements and frequency dependence of the irreducible self-energy. Our analysis shows that these corrections are included as semireducible and linked-disconnected diagrams, respectively, which are also found in a perturbation expansion of the electron binding energies of the equation-of-motion coupled-cluster methods. The rate of convergence of the electron binding energies with respect to n and its acceleration by Padé approximants are also discussed.

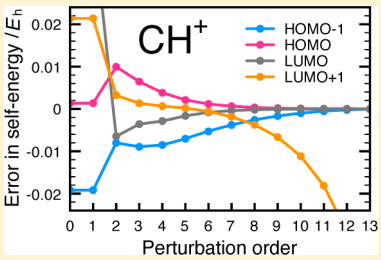

1. INTRODUCTION

The ability to perform calculations of a systematic electron-correlation method at any rank and to obtain reliable reference data is critical for the subsequent development of the method into an efficient algorithm for practical applications. Knowles et al.[1] reported a general-order Møller−Plesset perturbation (MP) method, which solved its recursive equation for perturbation corrections to wave functions expanded as linear combinations of Slater determinants using a full configuration-interaction (FCI) algorithm.[2] Three groups[3−5] independently developed a general-order coupled-cluster (CC) method, also adopting the determinant-based FCI algorithm. This was immediately extended[6,7] to excited, electron-detached, and electron-attached states in the equation-of-motion (EOM) CC formalism.[8,9] Truncated configuration-interaction (CI) methods[2] for any type of states are inherently general-order methods, if the determinant-based algorithm is used.

One-electron many-body Green's function (GF) or electron propagator theory[10−19] also forms a systematic series of approximations. It computes electron-detachment and -attachment energies (collectively, electron binding energies) directly from the Dyson equation and not as energy differences. It is rigorously (i.e., diagrammatically) size-consistent and is thus applicable to solids. Given the attention paid to energy bands (which are electron binding energies as a function of the wave vector) in characterizing the properties and functions of advanced materials, GF theory is of crucial importance today. Quasiparticle (i.e., electron-correlated) energy bands of one-dimensional solids obtained with the second-order GF (GF2) method were reported[20−23] to be considerably more accurate than those obtained from the Hartree−Fock (HF) method. They can furthermore be made systematically more accurate by raising the perturbation order, unlike the energy bands obtained from density-functional approximations, which also tend to be unreliable.[24]

However, GF theory has thus far resisted a general-order implementation for several reasons. First, GF theory is almost always defined diagrammatically, i.e., in the language that is fundamentally incongruous to the determinant-based (i.e., CI-like) implementation. The same applies to the superoperator algebra[10,13,25] and to the Dyson−Gell-Mann−Low time-dependent perturbation theory derivation.[26,27] Second, GF theory is based on the Dyson equation (not the Schrödinger equation), and its formulation does not explicitly refer to wave functions, which a determinant-based algorithm stores and manipulates. Whereas two of the authors as well as others implemented partial and full third-order[28−39] and partial and full fourth-order self-energies[30,40−42] both within the GF and EOM frameworks, higher-order GF methods are yet to be developed and detailed knowledge about convergence is lacking. To obtain these, a general-order implementation, which can generate reliable reference data up to high orders, is paramount in view of the fact that there are many more diagrams in the nth-order GF (GFn) method than in the nth-order MP (MPn) method (e.g., 18 Hugenholtz diagrams in GF3 versus three in MP3).

In this article, we report a general-order GF method with a determinant-based algorithm and document electron binding energies including up to nth-order self-energies $(0 \le n \le 30)$ for several small molecules. Here, the nth-order self-energy is

Received: January 4, 2015
Published: February 20, 2015

DOI: 10.1021/acs.jctc.5b00005
J. Chem. Theory Comput. 2015, 11, 1595−1606

defined as the difference in the MPn energy between the N- and $(N \pm 1)$-electron systems, all of which are described with the HF orbitals and orbitals energies of the N-electron system. These MPn energies are, in turn, calculated at any n by the general-order MP method of Knowles et al.[1] We call this procedure ΔMPn, which must not be confused with the simple difference in MPn energies obtained with the HF orbitals individually determined for N- and $(N \pm 1)$-electron systems; nowhere in a ΔMPn calculation for a closed-shell molecule is a HF calculation of an open-shell molecule performed, which tends to suffer from spin contamination.[43] While ΔMPn implemented algebraically was used by Chong et al.[44−46] in their analysis of GFn at low orders, little is known about its behavior at $n > 3$.

For $0 \leq n \leq 3$, the electron binding energies obtained from ΔMPn are identified as the values determined with the self-energies in the diagonal approximation and evaluated at the HF orbital energies, namely, in the frequency-independent approximation. However, as $n \to \infty$, they converge at the exact basis-set values obtained with FCI or with the full GF method using the exact self-energy, which is nondiagonal and frequency-dependent. This suggests that ΔMPn includes the perturbation corrections due to the off-diagonal elements and frequency dependence of the irreducible self-energy exactly at $n = \infty$. These corrections are shown to be represented as semireducible and linked-disconnected diagrams, respectively, according to our analysis of low-order examples. While it is well-known that a perturbation expansion of the nondiagonal, frequency-dependent self-energy is convergent at exactness, we show that a perturbation expansion of the diagonal, frequency-independent self-energy is also convergent at the same limit insofar as these new classes of diagrams are taken into account. We furthermore show that a perturbation expansion of the electron binding energies obtained from the EOM-CC methods also contains the same classes of diagrams.

Hence, ΔMPn suggests an alternative perturbation approach to GF theory with a potentially streamlined algorithm, which does not involve diagonalization or self-consistent solution of the Dyson equation, while converging at the exact limits. Its drawbacks are the reduced applicability to just Koopmans-like final states and the inability to resist divergence, as this ability is conferred by a frequency-dependent self-energy. In this work, therefore, we also numerically monitor the electron binding energies of ΔMPn for a few molecules as a function of n to examine their convergence rates and whether the correct converged limits can be deduced from divergent series. We show that Padé approximants can extrapolate the correct converged limit within a few mE_h from divergent series, although it proves to be less effective in accelerating the convergence rates elsewhere.

2. THEORY

Throughout this article, atomic units are adopted. We use i, j, k, l, m, and n (a, b, c, and d) to label occupied (virtual) orbitals in the spin-restricted HF determinant of an N-electron system in its ground state (N is an even number) and p, q, r, and s to signify either type of orbitals. We furthermore employ x and y to designate an appropriate type of orbitals from which an electron is removed or added. Unless otherwise noted, all orbitals refer to canonical HF spin-orbitals.

2.1. One-Electron Many-Body Green's Function theory.

The central equation of GF theory is the Dyson equation[10−19]

$$\boldsymbol{G}(\omega) = \boldsymbol{G}_0(\omega) + \boldsymbol{G}_0(\omega)\,\boldsymbol{\Sigma}(\omega)\,\boldsymbol{G}(\omega) \tag{1}$$

which relates the exact one-electron Green's function, $\boldsymbol{G}(\omega)$, with the zeroth-order (in our case, HF) one-electron Green's function, $\boldsymbol{G}_0(\omega)$, through Dyson self-energy, $\boldsymbol{\Sigma}(\omega)$. In a finite basis set, they all are L-by-L matrices, where L is the number of orbitals, and are dependent on frequency, ω.

In the basis of the HF orbitals, the matrix elements of the exact and HF Green's functions are given, respectively, by

$$\{\mathbf{G}(\omega)\}_{xy} = \sum_n \frac{\langle {}^N\Psi_0|\hat{x}^\dagger|{}^{N-1}\Psi_n\rangle\langle {}^{N-1}\Psi_n|\hat{y}|{}^N\Psi_0\rangle}{\omega - ({}^NE_0 - {}^{N-1}E_n)} + \sum_n \frac{\langle {}^N\Psi_0|\hat{y}|{}^{N+1}\Psi_n\rangle\langle {}^{N+1}\Psi_n|\hat{x}^\dagger|{}^N\Psi_0\rangle}{\omega - ({}^{N+1}E_n - {}^NE_0)} \tag{2}$$

$$\{\mathbf{G}_0(\omega)\}_{xy} = \frac{\delta_{xy}}{\omega - \epsilon_x} \tag{3}$$

where $\hat{x}^\dagger$ creates an electron in the xth orbital, $\hat{x}$ annihilates the same, ${}^N\Psi_n$ is the exact wave function of the nth state ($n = 0$ being the ground state) of the N-electron system, ${}^NE_n$ is the exact energy of the same state, and ϵ_x is the energy of the xth orbital.

Hence, $\boldsymbol{G}(\omega)$ has poles at exact negative electron-detachment energies $({}^NE_0 - {}^{N-1}E_n)$ and exact negative electron-attachment energies $({}^{N+1}E_n - {}^NE_0)$, whereas $\boldsymbol{G}_0(\omega)$ has poles at the energies of the HF orbitals, which are related to the electron-detachment and -attachment energies of HF theory in the Koopmans approximation. A bound anionic state is thus often foreshadowed by a negative, virtual, HF orbital energy.

Multiplying eq 1 with $\boldsymbol{G}_0^{-1}(\omega)$ from the left and $\boldsymbol{G}^{-1}(\omega)$ from the right, we obtain the inverse Dyson equation

$$\boldsymbol{G}_0^{-1}(\omega) = \boldsymbol{G}^{-1}(\omega) + \boldsymbol{\Sigma}(\omega) \tag{4}$$

Since $\boldsymbol{G}(\omega)$ diverges at an exact electron binding energy, say ω

$$0 = \det\{\boldsymbol{G}^{-1}(\omega)\} = \det\{\boldsymbol{G}_0^{-1}(\omega) - \boldsymbol{\Sigma}(\omega)\} \tag{5}$$

One way to solve eq 5 is to use a new set of orbitals that brings $\boldsymbol{G}^{-1}(\omega)$ into a diagonal form. Since

$$\boldsymbol{G}_0^{-1}(\omega) = \omega\mathbf{1} - \boldsymbol{\epsilon} \tag{6}$$

with $\{\boldsymbol{\epsilon}\}_{xy} = \delta_{xy}\epsilon_x$ in the basis of the HF orbitals, the new orbitals diagonalize $\boldsymbol{\epsilon} + \boldsymbol{\Sigma}(\omega)$ also. Let $\tilde{\Sigma}_x(\omega)$ be the xth diagonal element of $\boldsymbol{\epsilon} + \boldsymbol{\Sigma}(\omega)$ in this new basis. Equation 5 then simplifies to

$$0 = \prod_x \{\omega - \tilde{\Sigma}_x(\omega)\} \tag{7}$$

or

$$\omega = \tilde{\Sigma}_x(\omega) \tag{8}$$

which is to be solved for ω by bringing it to self-consistency between the left- and right-hand sides (whereupon the xth orbital becomes a Dyson orbital).

To distinguish from approximate solutions to be discussed below, we call the solution of the above equation the non-diagonal, self-consistent solution. The recursive structure of the inverse Dyson equation allows a single eq 8 to have multiple roots, corresponding not only to the fundamental (Koopmans) but also to satellite (shakeup) transitions.

In the diagonal approximation, the off-diagonal elements of $\boldsymbol{G}^{-1}(\omega)$ [thus $\boldsymbol{\Sigma}(\omega)$] in the basis of the HF orbitals are neglected. Then, eq 5 reduces to

$$0 = \prod_x \{\omega - \epsilon_x - \Sigma_x(\omega)\} \tag{9}$$

DOI: 10.1021/acs.jctc.5b00005
J. Chem. Theory Comput. 2015, 11, 1595−1606

where $\Sigma_x(\omega)$ is the xth diagonal element of $\mathbf{\Sigma}(\omega)$. This leads to a recursive equation

$$\omega = \epsilon_x + \Sigma_x(\omega) \tag{10}$$

which is, again, to be solved for ω, making the left- and right-hand sides self-consistent. We call this the diagonal approximation.[47]

A simpler alternative to seeking self-consistent solutions is to evaluate the self-energy at $\omega = \epsilon_x$, that is

$$\omega = \epsilon_x + \Sigma_x(\epsilon_x) \tag{11}$$

We call this method the diagonal, frequency-independent (ω-independent) approximation.[47] This may be justified when ϵ_x is sufficiently far from any of the poles of $\Sigma_x(\omega)$, where the latter is nearly constant with ω. It gives the energies of the fundamental transitions only.

2.2. Feynman−Goldstone Diagrams. The self-energy in the basis of the HF orbitals is expanded into a diagrammatic perturbation series.[26,27] In the diagonal approximation, we can write

$$\omega^{(n)} = \sum_{m=0}^{n} \Sigma_x^{(m)}(\omega) \tag{12}$$

where $\omega^{(n)}$ is the electron binding energy in the nth-order perturbation theory and $\Sigma_x^{(m)}(\omega)$ is the mth-order perturbation correction to the self-energy. The Møller−Plesset partitioning of the Hamiltonian, $\hat{H} = \hat{H}_0 + \hat{V}$, is used, where $\hat{H}_0$ is the sum of the Fock operators and $\hat{V}$ is the fluctuation potential. This partitioning is consistent with $\mathbf{G}_0(\omega)$ being defined by HF theory. Hence, $\Sigma_x^{(0)}(\omega) = \epsilon_x$.

The mth-order correction to the self-energy, $\Sigma_x^{(m)}$, is the sum of contributions from all Feynman−Goldstone diagrams with m interaction ($\hat{V}$) vertexes that are linked, irreducible, and open with exactly two external edges or "stubs".[26,27] These diagrams are then interpreted expediently according to the established rules[26,27] into algebraic expressions of $\Sigma_x^{(m)}$. These rules are rigorously derivable by the Dyson−Gell-Mann−Low time-dependent perturbation theory[26,27] and are mathematically equivalent to the superoperator algebra.[10,13,18,25] The diagrammatic method, however, can provide unique, graphical information about size consistency of GF theory,[48−50] the recursive structure of the Dyson equation,[26,50] the concept of edge insertion,[50−52] etc.

Figure 1 draws the MP2 energy diagram as diagram A. The closed, linked nature of this diagram ensures the extensivity of the

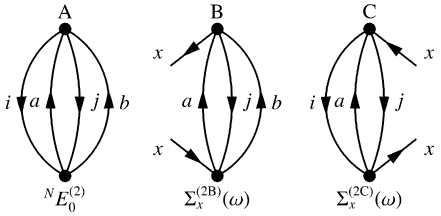

Figure 1. MP2 energy diagram and second-order diagonal self-energy diagrams in the Hugenholtz style.

MP2 energy.[48,49,53] Specifically, each four-edge vertex (representing a two-electron integral) contributes a factor of V^{-1} to the volume (V) dependence of the diagram, and each independent internal edge (a line connecting two vertexes), a factor of V. Of the four internal edges in diagram A, only three are independent with the fourth determined by the momentum conservation law. Together, diagram A scales as $V^{-2}V^3 = V$ and is thermodynamically extensive.

Self-energy diagrams can be generated by "cutting an edge" of closed diagrams with the same order (plus additional ones, in some instances[31]) in all topologically distinct ways. Cutting the ith edge of diagram A, we obtain self-energy diagram B. Cutting the bth edge spawns self-energy diagram C. The edge that has been cut becomes two external edges, which do not contribute to the V dependence of the diagram. Diagrams B and C, therefore, scale as $V^{-2}V^2 = V^0$ and represent thermodynamically intensive quantities.

These diagrams are directly translated to algebraic expressions according to the established rules found in, e.g., Mattuck.[26] For future use, we translate diagrams B and C into algebraic forms

$$\Sigma_x^{(2B)}(\omega) = \frac{1}{2}\sum_{j,a,b} \frac{\langle xj||ab\rangle\langle ab||xj\rangle}{\omega + \epsilon_j - \epsilon_a - \epsilon_b} \tag{13}$$

$$\Sigma_x^{(2C)}(\omega) = \frac{1}{2}\sum_{i,j,a} \frac{\langle ij||ax\rangle\langle ax||ij\rangle}{\omega + \epsilon_a - \epsilon_i - \epsilon_j} \tag{14}$$

Figure 2 shows an example of an unlinked diagram. An unlinked diagram is a special case of a disconnected diagram and

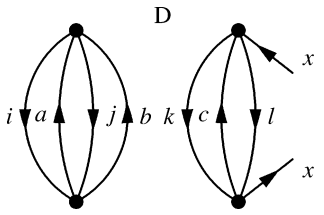

Figure 2. An unlinked fourth-order diagonal self-energy diagram in the Hugenholtz style.

contains at least one closed subdiagram. Such diagrams must be excluded because they have nonphysical size dependence. The algebraic interpretation of an unlinked diagram is the product of the interpretations of the subdiagrams. The left subdiagram of diagram D is closed and scales as V^1, whereas the right one scales as V^0. As a whole, diagram D displays V^1 dependence, which is incorrect as a self-energy diagram.

Figure 3 is an example of a reducible diagram, characterized by one or more articulation edges. An articulation edge is the one

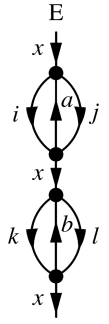

Figure 3. A reducible fourth-order diagonal self-energy diagram in the Hugenholtz style.

whose removal leaves the diagram disconnected. Reducible diagrams are also barred from the self-energy in the diagonal approximation because they are already included owing to the

DOI: 10.1021/acs.jctc.5b00005
J. Chem. Theory Comput. 2015, 11, 1595−1606

recursive structure of the Dyson equation and their explicit inclusion results in double counting of one and the same diagram.

$$\{\boldsymbol{G}(\omega)\}_{xx} = \{\boldsymbol{G}_0(\omega)\}_{xx} + \{\boldsymbol{G}_0(\omega)\}_{xx}\,\Sigma_x(\omega)\{\boldsymbol{G}_0(\omega)\}_{xx} + \{\boldsymbol{G}_0(\omega)\}_{xx}\,\Sigma_x(\omega)\{\boldsymbol{G}_0(\omega)\}_{xx} \times \Sigma_x(\omega)\{\boldsymbol{G}_0(\omega)\}_{xx} + \ldots \quad (15)$$

For instance, diagram E is a part of the third term of the right-hand side, once diagram C is in the self-energy. Note that the external and articulation edges share the same label. If they do not, then this diagram accounts for a nonredundant contribution from the off-diagonal elements of the irreducible second-order self-energy and is no longer considered to be reducible. We call such diagrams semireducible.

2.3. ΔMP Method. Here, we introduce what we call the ΔMP*n* method, in which the *n*th-order "self-energy" (whose definition, as shown below, differs from the usual one) is obtained as the MP*n* energy difference between the *N*- and $(N \pm 1)$-electron systems.[44−47] The energies of the latter are calculated with the HF orbitals and orbital energies determined for the *N*-electron system. This ΔMP*n* approach provides well-defined formulas for electron binding energies at any order of perturbation theory, which are valid for Koopmans-like final states; it is alternative to methods using frequency-dependent self-energies, which require a pole search. In this work, the MP*n* energies with any value of *n* are obtained by the general-order MP method of Knowles et al.,[1] thus realizing an implementation of a general-order GF method having a FCI computational cost.

Let ${}^{M}\Psi_x^{(n)}$ and ${}^{M}E_x^{(n)}$ be the *n*th-order perturbation corrections to the wave function and energy of the *M*-electron state ($M = N$ or $N \pm 1$); ${}^{N\pm1}\Psi_x^{(n)}$ corresponds to the Koopmans-like final state in which an electron is added to or removed from the *x*th orbital and ${}^{N}\Psi_x^{(n)}$ to the ground state, where $x = 0$. They are determined by solving the recursive equations of the Rayleigh−Schrödinger perturbation theory (RSPT)

$${}^{M}\Psi_x^{(n)} = {}^{M}\hat{R}\hat{V}\,{}^{M}\Psi_x^{(n-1)} - {}^{M}\hat{R}\sum_{m=1}^{n} {}^{M}E_x^{(m)}\,{}^{M}\Psi_x^{(n-m)} \quad (16)$$

with the resolvent,

$${}^{M}\hat{R} = ({}^{M}E_x^{(0)} - \hat{H}_0)^{-1} \quad (17)$$

and

$${}^{M}E_x^{(n)} = \langle {}^{M}\Psi_x^{(0)}|\hat{V}|{}^{M}\Psi_x^{(n-1)}\rangle \quad (18)$$

for $n \geq 1$. We use the single determinant ${}^{M}\Phi_x$ as the initial (zeroth-order) wave function to commence the recursion, i.e., ${}^{M}\Psi_x^{(0)} = {}^{M}\Phi_x$, where ${}^{N}\Phi_0$ is the HF ground-state determinant and ${}^{N\pm1}\Phi_x$ is the determinant in which an electron is added to or removed from the *x*th orbital of ${}^{N}\Phi_0$. All of the orbitals entering these determinants, $\hat{H}$, $\hat{H}_0$, and $\hat{V}$ are the HF orbitals of the *N*-electron system.

We express each of $\{{}^{M}\Psi_x^{(n)}\}$ as a CI vector in the determinant basis, as described by Knowles and Handy.[2] It should be understood that the determinant contribution in ${}^{M}\Psi_x^{(n)}$ that causes a divergence in the resolvent, ${}^{M}\hat{R}$, is excluded.[54] The difference in the *n*th-order energy between *N*- and $(N \pm 1)$-electron cases gives an *n*th-order self-energy, that is

$$\Sigma_x^{(n)} = {}^{N}E_0^{(n)} - {}^{N-1}E_x^{(n)} \quad (19)$$

$$\Sigma_x^{(n)} = {}^{N+1}E_x^{(n)} - {}^{N}E_0^{(n)} \quad (20)$$

In eqs 19 and 20, we intentionally omitted the frequency argument of the self-energies. This is because whether they correspond to the frequency-independent one, $\Sigma_x^{(n)}(\epsilon_x)$, or the self-consistent one, $\Sigma_x^{(n)}(\omega)$, varies with *n*. Also, depending on *n*, the ΔMP*n* result may or may not be equal to the value obtained from the diagonal approximation of the irreducible self-energy. This fascinating observation is addressed and analyzed in the following.

At this stage, we note that the self-energies from ΔMP0 are well-known[47] to be the HF orbital energies

$$\Sigma_x^{(0)} = \epsilon_x \quad (21)$$

which are diagonal and independent of frequency. The ΔMP1 corrections to the self-energies are shown to be zero[47]

$$\Sigma_x^{(1)} = 0 \quad (22)$$

which are also diagonal and frequency-independent. It is also known[25,47] analytically that the corrections due to ΔMP2 are the second-order self-energies in the diagonal and frequency-independent approximations:

$$\Sigma_x^{(2)} = \Sigma_x^{(2B)}(\epsilon_x) + \Sigma_x^{(2C)}(\epsilon_x) \quad (23)$$

See eqs 13 and 14 for the definitions of the terms in the right-hand side.

2.4. Full GF Method. Using the determinant-based algorithm,[2] we additionally perform hole-particle FCI to obtain the exact electron binding energies within a basis set.[7] They correspond to the self-consistent solutions of the Dyson equation using the exact self-energy without the diagonal or frequency-independent approximation. They are used for comparison with the electron binding energies from ΔMP*n*. We also calculate the electron binding energies in the diagonal and/or frequency-independent treatment but without any further approximation (such as a finite-order perturbation approximation to the self-energy) by the procedure called "full GF" described below.

First, we use hole-particle FCI to obtain the exact ground-state energy and wave function of the *N*-electron system and all of the exact ground- and excited-state energies and wave functions of the $(N \pm 1)$-electron systems. Substituting them in eq 2, we obtain the *L*-by-*L* matrix of $\boldsymbol{G}(\omega)$ at any given ω. The computational machinery of acting $\hat{x}^{\dagger}$ and $\hat{y}$ on wave functions is furnished by the determinant-based algorithm.[2,7]

Next, we find a unitary matrix $\boldsymbol{U}(\omega)$ that diagonalizes $\boldsymbol{G}(\omega)$

$$\boldsymbol{U}^{\dagger}(\omega)\,\boldsymbol{G}(\omega)\,\boldsymbol{U}(\omega) = \boldsymbol{g}(\omega) \quad (24)$$

where $\boldsymbol{g}(\omega)$ is a diagonal matrix

$$\{\boldsymbol{g}(\omega)\}_{xy} = \delta_{xy} g_x(\omega) \quad (25)$$

In this new basis, the inverse Dyson equation (eq 5) is simplified to

$$0 = \det\{\boldsymbol{G}^{-1}(\omega)\} = \prod_x \frac{1}{g_x(\omega)} \quad (26)$$

or

$$0 = \frac{1}{g_x(\omega)} \quad (27)$$

for each *x*. The roots of this equation are the exact electron binding energies without the diagonal or frequency-independent approximation. It is confirmed that they agree with the results of hole-particle FCI.

DOI: 10.1021/acs.jctc.5b00005
J. Chem. Theory Comput. 2015, 11, 1595−1606

Table 1. Electron Binding Energies (in E_h) of BH (r_{BH} = 1.232 Å) Calculated with the STO-3G Basis Set[a]

method	algorithm	approximation	HOMO − 1	HOMO	LUMO[b]
HF	algebraic	diagonal, ω-independent	−0.57349	−0.24654	0.26994
GF0 = ΔMP0	determinant	ΔMP	−0.57349	−0.24654	0.26994
GF1 = ΔMP1	determinant	ΔMP	−0.57349	−0.24654	0.26994
GF2 = ΔMP2	determinant	ΔMP	−0.57656	−0.24400	0.26330
GF2	algebraic	diagonal, ω-independent	−0.57656	−0.24400	0.26330
GF2	algebraic	diagonal	−0.57649	−0.24407	0.26343
GF3 = ΔMP3	determinant	ΔMP	−0.57333	−0.24766	0.26724
GF3	algebraic	diagonal, ω-independent	−0.57333	−0.24766	0.26724
GF3	algebraic	diagonal	−0.57334	−0.24761	0.26732
GF30 = ΔMP30	determinant	ΔMP	−0.55487	−0.25700	0.27470
full GF	determinant	diagonal, ω-independent	−0.55010	−0.25837	0.27497
full GF	determinant	diagonal	−0.55326	−0.25737	0.27470
full GF = FCI	determinant	none	−0.55488	−0.25700	0.27470

[a]The lowest spatial orbital is kept frozen in the correlation treatment. The HF and FCI energies of the ground state are $-24.752788E_h$ and $-24.809629E_h$, respectively. [b]Doubly degenerate.

In the basis of the HF orbitals, $\boldsymbol{G}^{-1}(\omega)$ is obtained by the back transformation

$$\boldsymbol{G}^{-1}(\omega) = \boldsymbol{U}(\omega)\, \boldsymbol{g}^{-1}(\omega)\, \boldsymbol{U}^{\dagger}(\omega) \tag{28}$$

where $\boldsymbol{g}^{-1}(\omega)$ is the diagonal matrix whose xth diagonal element is $\{g_x(\omega)\}^{-1}$. The diagonal approximation neglects all off-diagonal elements of $\boldsymbol{G}^{-1}(\omega)$ in the basis of the HF orbitals. The inverse Dyson equation then becomes

$$0 = \prod_x \{\boldsymbol{U}(\omega)\, \boldsymbol{g}^{-1}(\omega)\, \boldsymbol{U}^{\dagger}(\omega)\}_{xx} \tag{29}$$

or

$$0 = \{\boldsymbol{U}(\omega)\, \boldsymbol{g}^{-1}(\omega)\, \boldsymbol{U}^{\dagger}(\omega)\}_{xx} \tag{30}$$

for each x. The roots of this equation correspond to the solutions of the Dyson equation using the exact self-energy in the diagonal approximation.

The electron binding energies in the diagonal, frequency-independent approximation are evaluated by

$$\omega = \epsilon_x + \Sigma_x(\epsilon_x) \tag{31}$$

$$= \epsilon_x - \{\boldsymbol{U}(\epsilon_x)\, \boldsymbol{g}^{-1}(\epsilon_x)\, \boldsymbol{U}^{\dagger}(\epsilon_x)\}_{xx} \tag{32}$$

3. RESULTS

The general-order GF (ΔMP) method was applied to the nth-order electron binding energies ($0 \le n \le 30$) of the two highest occupied spatial orbitals (HOMO − 1 and HOMO) and the lowest unoccupied spatial orbital (LUMO) of BH. The full GF method was also employed for the same orbitals of BH. The general-order GF (ΔMP) method also calculated the nth-order electron binding energies ($0 \le n \le 30$) of the HOMO − 1, HOMO, LUMO, and LUMO + 1 of CH^+ and C_2. The bond distances, basis sets used, and orbital spaces considered in the correlation treatment as well as the HF and FCI energies are given in the captions of the tables compiling those results.

Table 1 compares the results of determinant-based GFn (ΔMPn) with those from the corresponding algebraic implementations in the diagonal approximation at low orders ($0 \le n \le 3$). The determinant-based GFn program evaluates eqs 19 and 20, whereas the algebraic GFn program implements equations such as 13 and 14 in the case of n = 2. The algebraic GF3 program implements all 18 GF3 self-energy diagrams listed in Figure 6.2 of Jørgensen and Simons[13] and interpreted algebraically in Appendix D of Linderberg and Öhrn[10] and as eq 4.2 of Ferreira et al.[39] The table also lists the full GF results with and without the diagonal or frequency-independent approximation.

As mentioned above, it has been shown[47] analytically that the electron binding energies of ΔMP0 and ΔMP1 are the HF orbital energies. The electron binding energies of ΔMP2 are those in the diagonal, frequency-independent approximation. Sure enough, the determinant-based GFn (ΔMPn) results agree identically with the algebraic GFn results in the diagonal, frequency-independent approximation for $0 \le n \le 3$, mutually verifying their implementations. The self-consistent solutions of the Dyson equation (i.e., with the frequency-dependent self-energy) at the second and third orders, on the other hand, differ distinctly from the ΔMP2 or ΔMP3 values.

Remarkably, determinant-based GFn (ΔMPn) converges toward the exact solution, i.e., without the diagonal or frequency-independent approximation, as $n \to \infty$. Hence, ΔMPn uses the diagonal and frequency-independent approximations at low orders (at least $n \le 3$), but it eventually converges at the exact results without either approximation. Note that the full GF method with the diagonal and/or frequency-independent approximation does incur some errors and it is not that one or both of these approximations have no effect at $n = \infty$. In other words, ΔMPn takes into account the effects of the off-diagonal elements and frequency-dependence of the exact, irreducible self-energy without diagonalization or seeking self-consistent solutions of a recursive equation.

One trivial justification for this observation is that the MPn series for N- and $(N \pm 1)$-electron systems is individually convergent toward the exact total energies and, therefore, their differences should also converge at the exact self-energies, which are nondiagonal and frequency-dependent. In Sections 4.1 and 4.2, we offer more detailed, if speculative, explanations of this phenomenon. In short, ΔMPn includes the effects of the off-diagonal elements and frequency dependence of the self-energy as perturbation corrections and the first such nonzero corrections occur in fourth order (hence, the agreement with the diagonal, frequency-independent results at $n \le 3$). In other words, ΔMPn defines an alternative, converging, diagrammatic perturbation expansion of the self-energy. Unlike Dyson's original definition of the exact self-energy, however, this new

DOI: 10.1021/acs.jctc.5b00005
J. Chem. Theory Comput. 2015, 11, 1595−1606

Table 2. Electron Binding Energies (in E_h) of CH^+ (r_{CH} = 1.120 Å) with the 6-31G* Basis Set as a Function of Perturbation Order n[a]

n	HOMO − 1	HOMO	LUMO[b]	LUMO + 1	annotation
0	−1.25371	−0.87474	−0.32787	−0.04260	GF0 = HF
1	−1.25371	−0.87474	−0.32787	−0.04260	GF1 = HF
2	−1.24254	−0.86615	−0.37798	−0.06077	GF2 = ΔMP2
3	−1.24346	−0.86966	−0.37510	−0.06265	GF3 = ΔMP3
4	−1.24304	−0.87227	−0.37437	−0.06332	GF4 = ΔMP4
5	−1.24158	−0.87398	−0.37315	−0.06379	GF5 = ΔMP5
6	−1.23985	−0.87493	−0.37231	−0.06458	GF6 = ΔMP6
7	−1.23833	−0.87546	−0.37191	−0.06583	GF7 = ΔMP7
8	−1.23712	−0.87575	−0.37169	−0.06773	GF8 = ΔMP8
9	−1.23620	−0.87591	−0.37158	−0.07064	GF9 = ΔMP9
10	−1.23554	−0.87600	−0.37153	−0.07513	GF10 = ΔMP10
11	−1.23508	−0.87604	−0.37151	−0.08213	GF11 = ΔMP11
12	−1.23478	−0.87607	−0.37150	−0.09308	GF12 = ΔMP12
13	−1.23459	−0.87608	−0.37150	−0.11029	GF13 = ΔMP13
14	−1.23448	−0.87609	−0.37150	−0.13739	GF14 = ΔMP14
15	−1.23442	−0.87610	−0.37150	−0.18011	GF15 = ΔMP15
16	−1.23440	−0.87610	−0.37150	−0.24746	GF16 = ΔMP16
17	−1.23440	−0.87610	−0.37150	−0.35371	GF17 = ΔMP17
18	−1.23441	−0.87610	−0.37151	−0.52129	GF18 = ΔMP18
19	−1.23443	−0.87610	−0.37151	−0.78560	GF19 = ΔMP19
20	−1.23445	−0.87610	−0.37151	−1.20242	GF20 = ΔMP20
30	−1.23453	−0.87610	−0.37151	−107.692	GF30 = ΔMP30
∞	−1.23453	−0.87610	−0.37151	−0.06398	FCI[c]
	−1.24588	−0.87876	−0.37301	−0.06250	CCSD[d]
	−1.23505	−0.87614	−0.37179	−0.06374	CCSDT[d]
	−1.23453	−0.87610	−0.37151	−0.06393	CCSDTQ[d]

[a]The lowest and highest spatial orbitals are kept frozen in the correlation treatment. The HF and FCI energies of the ground state are −37.895388E_h and −37.990913E_h, respectively. [b]Doubly degenerate. [c]CI(4h-3p) for HOMO − 1 and HOMO and CI(4h-5p) for LUMO and LUMO + 1. [d]IP-EOM-CCSD(2h-1p), IP-EOM-CCSDT(3h-2p), or IP-EOM-CCSDTQ(4h-3p) for HOMO − 1 and HOMO and EA-EOM-CCSD(1h-2p), EA-EOM-CCSDT(2h-3p), or EA-EOM-CCSDTQ(3h-4p) for LUMO and LUMO + 1. See also Hirata et al.[7]

expansion is limited to Koopmans-like electron binding energies and can be divergent.

Table 2 lists the electron binding energies of CH^+ up to thirtieth order. The errors from the exact (FCI) electron binding energies are plotted in Figure 4. The results at n = 0 and 1 are equal to the HF values and the first nonzero correlation corrections occur at n = 2, which are substantial. The corrections from $n \geq 3$ are more incremental and progressively smaller, forming rather smoothly converging series, unless they diverge as they do for LUMO + 1. We do not necessarily observe "staircase" convergence behavior for MPn, although the results of C_2 (see below) do display oscillatory convergence.

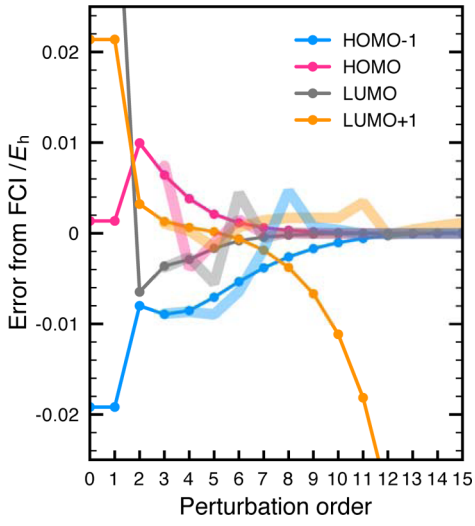

Figure 4. Convergence of the electron binding energies of CH^+ with the perturbation order (Table 2). The thick, semitransparent lines are the Padé approximants of the series with the same color (Table 3).

When the electron binding energies converge as $n \to \infty$, again, they do so at the exact values obtained by solving the Dyson equation self-consistently and without the diagonal approximation. From this calculation, it is unknown whether or to what extent these approximations slow the convergence, except for LUMO + 1, which we now discuss.

The electron binding energies of LUMO + 1 show a sign of divergence. Generally, the higher- or lower-lying the orbitals are and the higher the perturbation order is, the greater the chance of encountering this problem. For instance, the denominators in the algebraic second-order self-energy expression[10,13,47] in the diagonal and frequency-independent approximations (see eqs 13 and 14) cannot vanish when

$$\epsilon_{\mathrm{HOMO}} - E_g < \epsilon_x < \epsilon_{\mathrm{LUMO}} + E_g \tag{33}$$

where ϵ_{HOMO} and ϵ_{LUMO} are the HF energies of the HOMO and LUMO and $E_g = \epsilon_{\mathrm{LUMO}} - \epsilon_{\mathrm{HOMO}}$. For orbitals that satisfy this condition, the second-order self-energies are not divergent. All of the orbitals (including LUMO + 1) in Table 2 satisfy this condition and hence the calculated second-order electron binding energies are indeed reasonable. However, with increasing order,

DOI: 10.1021/acs.jctc.5b00005
J. Chem. Theory Comput. 2015, 11, 1595−1606

the radius of convergence contracts, ultimately causing the nonconvergence of LUMO + 1.[43,55,56]

One way to rectify the nonconvergence is to use Padé approximants, which require only a series with a minimum of two members. Table 3 compiles the extrapolated self-energies by $[M,M-1]$or $[M,M]$ Padé approximants, obtained using the formulas given by Laidig et al.[57] For convergent series, that is, for HOMO−1, HOMO, and LUMO, the clear benefit of Padé approximants appears only at high orders such as $n \geq 9$ (Figure 4), where the order (n) is defined as the highest-order self-energy needed for the extrapolation, i.e., $2M+1$ for $[M,M-1]$ and $2M+2$ for $[M,M]$. For LUMO + 1, Padé approximants can bring the nonconvergent series into a rapidly convergent one within a few mE_h of the exact value across a range of Padé orders, i.e., $3 \leq n \leq 30$.

Table 3. Padé Approximants of the Electron Binding Energies (in E_h) of CH^+[a]

Padé	n[b]	HOMO − 1	HOMO	LUMO	LUMO + 1
[1,0]	3	−1.24339	−0.86864	−0.37526	−0.06287
[1,1]	4	−1.24317	−0.87994	−0.37412	−0.06369
[2,1]	5	−1.24347	−0.87712	−0.37701	−0.06554
[2,2]	6	−1.24093	−0.87458	−0.36704	−0.06331
[3,2]	7	−1.23626	−0.87611	−0.37201	−0.06253
[3,3]	8	−1.22984	−0.87610	−0.37139	−0.06225
[4,3]	9	−1.23385	−0.87610	−0.37148	−0.06226
[4,4]	10	−1.23412	−0.87610	−0.37149	−0.06225
[5,4]	11	−1.23457	−0.87610	−0.37150	−0.06057
[5,5]	12	−1.23452	−0.87610	−0.37157	−0.06415
[6,5]	13	−1.23452	−0.87610	−0.37151	−0.06356
[6,6]	14	−1.23452	−0.87610	−0.37151	−0.06317
[7,6]	15	−1.23453	−0.87610	−0.37151	−0.06281
[7,7]	16	−1.23454	−0.87610	−0.37151	−0.06324
[8,7]	17	−1.23454	−0.87610	−0.37151	−0.06363
[8,8]	18	−1.23453	−0.87610	−0.37148	−0.06381
[9,8]	19	−1.23452	−0.87610	−0.37151	−0.06394
[9,9]	20	−1.23455	−0.87610	−0.37151	−0.06226
[14,14]	30	−1.23453	−0.87610	−0.37151	−0.06399

[a]See also Table 2. [b]The highest-order self-energy used is as follows: $n = 2M+1$ for $[M,M-1]$ Padé and $n = 2M+2$ for $[M,M]$ Padé.

The electron binding energies obtained from the ionization-potential and electron-attached EOM-CC (IP-EOM-CC and EA-EOM-CC) methods[7−9,58,59] are rapidly convergent with the rank of the excitation operators included in the formalisms. Judging from the results for HOMO and LUMO, IP-EOM-CCSD and EA-EOM-CCSD seem able to achieve comparable accuracy with ΔMP4 or ΔMP5. See Section 4.3 for a comparative perturbation analysis of IP-EOM-CCSD and ΔMPn.

Table 4 lists the electron binding energies of C_2. C_2 has a greater degree of nondynamical correlation (caused by near degeneracy of partially filled $2\sigma_g$, $1\pi_u$, and $3\sigma_g$ orbitals[59]) than BH or CH^+, but the convergence is reasonably rapid. Unlike CH^+, however, the convergence is oscillatory, as seen in Figure 5, rendering some of the low-order self-energies (such as at $n = 2$ or 3) rather poor. It also seems to make Padé approximants less effective. It is interesting to note that the IP-EOM-CC series for this molecule is also oscillatory with the CC rank.[7]

4. DISCUSSION

4.1. Corrections Due to the Off-Diagonal Elements of the Self-Energy. The ΔMPn results agree with the electron binding energies in the diagonal approximation at $n \leq 3$, but they converge at the exact, nondiagonal values at $n = \infty$. This is because, at $n \geq 4$, ΔMPn includes perturbation corrections due to

Table 4. Electron Binding Energies (in E_h) of C_2 (r_{CC} = 1.262 Å) with the 6-31G Basis Set as a Function of Perturbation Order n[a]

n	HOMO − 1	HOMO[b]	LUMO	LUMO + 1[b]	annotation
0	−0.51235	−0.44816	−0.10057	0.16318	GF0 = HF
1	−0.51235	−0.44816	−0.10057	0.16318	GF1 = HF
2	−0.54478	−0.47645	−0.06928	0.18099	GF2 = ΔMP2
3	−0.51450	−0.41986	−0.07715	0.17051	GF3 = ΔMP3
4	−0.54183	−0.45567	−0.05745	0.18290	GF4 = ΔMP4
5	−0.53347	−0.43824	−0.05849	0.17931	GF5 = ΔMP5
6	−0.53823	−0.44338	−0.05408	0.18287	GF6 = ΔMP6
7	−0.54022	−0.44412	−0.04937	0.18452	GF7 = ΔMP7
8	−0.53866	−0.44205	−0.05095	0.18382	GF8 = ΔMP8
9	−0.54150	−0.44508	−0.04659	0.18638	GF9 = ΔMP9
10	−0.54028	−0.44378	−0.04803	0.18534	GF10 = ΔMP10
11	−0.54117	−0.44500	−0.04626	0.18666	GF11 = ΔMP11
12	−0.54123	−0.44524	−0.04638	0.18644	GF12 = ΔMP12
13	−0.54098	−0.44523	−0.04622	0.18671	GF13 = ΔMP13
14	−0.54136	−0.44580	−0.04591	0.18684	GF14 = ΔMP14
15	−0.54105	−0.44563	−0.04607	0.18685	GF15 = ΔMP15
16	−0.54117	−0.44588	−0.04595	0.18685	GF16 = ΔMP16
17	−0.54111	−0.44589	−0.04597	0.18695	GF17 = ΔMP17
18	−0.54104	−0.44587	−0.04604	0.18680	GF18 = ΔMP18
19	−0.54108	−0.44595	−0.04599	0.18694	GF19 = ΔMP19
20	−0.54100	−0.44588	−0.04607	0.18680	GF20 =ΔMP20
30	−0.54097	−0.44582	−0.04611	0.18679	GF30 = ΔMP30
∞	−0.54097	−0.44582	−0.04611	0.18679	FCI[c]

[a]The two lowest and two highest spatial orbitals are kept frozen in the correlation treatment. The HF and FCI energies of the ground state are −75.349114E_h and −75.609844E_h, respectively. [b]Doubly degenerate. [c]CI(8h-7p) for HOMO − 1 and HOMO and CI(8h-9p) for LUMO and LUMO + 1.

DOI: 10.1021/acs.jctc.5b00005
J. Chem. Theory Comput. 2015, 11, 1595−1606

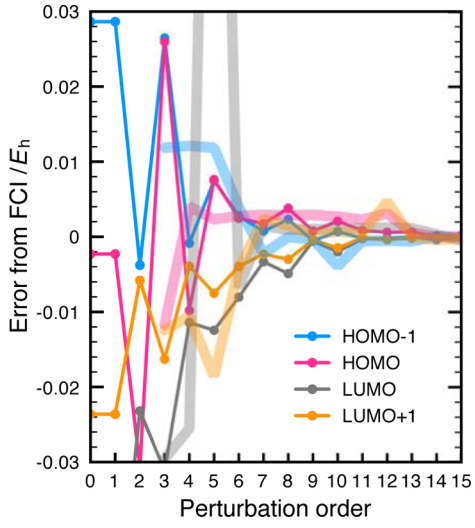

Figure 5. Same as Figure 4 but for C_2.

the off-diagonal elements of the irreducible self-energy. The following is an illustration of how this occurs at $n = 4$.

Equation 7 indicates that the exact electron binding energies are the eigenvalues of $\boldsymbol{\epsilon} + \boldsymbol{\Sigma}(\omega)$. Considering $\boldsymbol{\epsilon}$ of this matrix the zeroth-order part and $\boldsymbol{\Sigma}(\omega)$ the perturbation, the xth eigenvalue (ω_x) of $\boldsymbol{\epsilon} + \boldsymbol{\Sigma}(\omega)$ is expanded in a perturbation series

$$\omega_x = \epsilon_x + \Sigma_x(\omega) + \sum_{y \neq x} \frac{\{\boldsymbol{\Sigma}(\omega)\}_{xy}\{\boldsymbol{\Sigma}(\omega)\}_{yx}}{\epsilon_x - \epsilon_y} + \ldots \tag{34}$$

Substituting $\omega = \epsilon_x$ in the right-hand side, we obtain a perturbation formula for ω_x in the nondiagonal, frequency-independent approximation. The truncation of this equation after the second term amounts to the diagonal approximation (eq 11). The third term is, therefore, the leading-order contribution from the off-diagonal elements of the irreducible self-energy. The restriction in the summation index, $y \neq x$, in this term is related to the removal of reducible diagrams such as E in Figure 3. This diagram has the shared label (x) between the external and articulation edges, which corresponds to the excluded value of the index $(y = x)$ in eq 34, which, if retained, causes a divergence.

Figure 6 illustrates how diagrammatic contributions from the third term of eq 34 are included in ΔMP4. Diagram F is an MP4

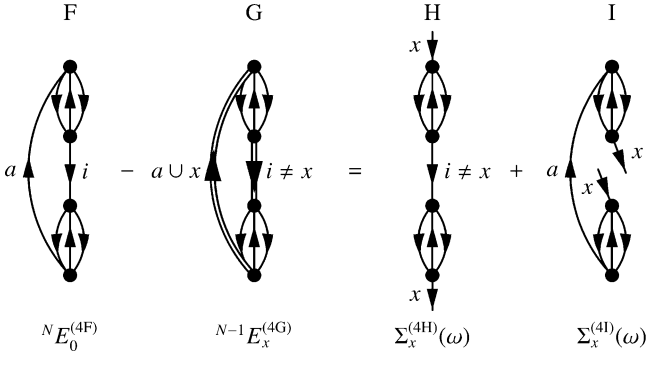

Figure 6. MP4 energy diagrams of the N- and $(N-1)$-electron systems (diagrams F and G) and the corresponding semireducible fourth-order diagonal self-energy diagrams (diagrams H and I) obtained as their differences. The double-lined edges in diagram G have different ranges of edge indexes between N- and $(N-1)$-electron systems.

energy diagram from which reducible diagrams can be generated upon cutting either the ath or ith edge. Diagram G is the same diagram for the $(N-1)$-electron system with the vacant xth orbital. Since, in the latter, the xth orbital is classified as a virtual orbital, the ath orbital index in diagram G runs over all virtual orbitals in ${}^{N}\Phi_0$ as well as x, whereas the range of the ith index excludes x. Hence, the differences between diagrams F and G give rise to self-energy diagrams H and I in ΔMP4. They are identified as semireducible diagrams and are concatenation of two second-order irreducible self-energy diagrams with an articulation edge. They are not reducible diagrams such as E because the label of the articulation edge differs from that of the external edges in each case. In fact, the combined range of the articulation-edge index in diagrams H and I is all orbitals except x, in agreement with the third term in eq 34.

In short, semireducible diagrams such as H and I account for the effect of the off-diagonal elements of the irreducible self-energy. Figure 6 furthermore indicates that the lowest order at which semireducible diagrams arise and hence the diagonal approximation and ΔMPn differ from each other is four (recall that the first-order self-energy is zero). This is consistent with the observation that ΔMPn $(0 \leq n \leq 3)$ agree with the results obtained in the diagonal approximation.

4.2. Corrections Due to the Frequency Dependence of the Self-Energy. The ΔMPn method yields electron binding energies in the frequency-independent approximation at $0 \leq n \leq 3$, but it gives the self-consistent solutions of the Dyson equation with the frequency-dependent self-energy at $n = \infty$. It thus follows that ΔMPn includes perturbation corrections due to the frequency dependence of the self-energy. Such corrections may be written in a Taylor series of eq 10, which reads

$$\omega_x^{(n)} = \epsilon_x + \sum_{m=2}^{n} \Sigma_x^{(m)}(\epsilon_x) + \sum_{m=1}^{n-1} \left.\frac{\partial \Sigma_x^{(n-m)}(\omega)}{\partial \omega}\right|_{\epsilon_x} \Sigma_x^{(m)}(\epsilon_x) + \frac{1}{2}\sum_{l=1}^{n-2}\sum_{m=1}^{n-l-1} \left.\frac{\partial^2 \Sigma_x^{(n-l-m)}(\omega)}{\partial \omega^2}\right|_{\epsilon_x} \Sigma_x^{(l)}(\epsilon_x)\Sigma_x^{(m)}(\epsilon_x) + \ldots \tag{35}$$

Since $\Sigma_x^{(1)}(\omega) = 0$, the first nonvanishing contribution occurs at $n = 4$ or, more specifically

$$\omega_x^{(4)} = \epsilon_x + \sum_{m=2}^{4} \Sigma_x^{(m)}(\epsilon_x) + \left.\frac{\partial \Sigma_x^{(2)}(\omega)}{\partial \omega}\right|_{\epsilon_x} \Sigma_x^{(2)}(\epsilon_x) \tag{36}$$

This is consistent with the observation that the third- and lower-order self-energies of ΔMPn are in the frequency-independent approximation. Using eqs 13 and 14, we find

$$\left.\frac{\partial \Sigma_x^{(2)}(\omega)}{\partial \omega}\right|_{\epsilon_x} = -\frac{1}{2}\sum_{j,a,b} \frac{\langle xj||ab\rangle\langle ab||xj\rangle}{(\epsilon_x + \epsilon_j - \epsilon_a - \epsilon_b)^2} - \frac{1}{2}\sum_{i,j,a} \frac{\langle ij||ax\rangle\langle ax||ij\rangle}{(\epsilon_x + \epsilon_a - \epsilon_i - \epsilon_j)^2} \tag{37}$$

Hence, the corrections due to the last term of eq 36 is diagrammatically represented partially as Figure 7. It is disconnected, but still linked (since there is no closed subdiagram), reflecting the simple product nature of the last term in eq 36. It does not, however, destroy the size consistency of ΔMP4 for the following reason: Each subdiagram in diagram J is isomorphic to

DOI: 10.1021/acs.jctc.5b00005
J. Chem. Theory Comput. 2015, 11, 1595−1606

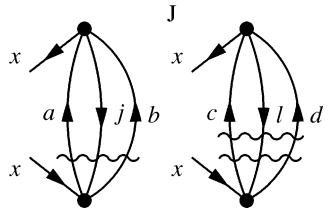

Figure 7. A linked-disconnected (thus size-consistent) fourth-order self-energy diagram. A wiggly line is a resolvent line.[54] Since the algebraic interpretation of a disconnected diagram is the simple product of the interpretations of subdiagrams, the chronological order of vertexes in different subdiagrams is immaterial and left unspecified.

a self-energy diagram and scales as V^0, rendering diagram J as a whole scale as $V^0V^0 = V^0$ (intensive). In other words, diagram J satisfies the intensive diagram theorem[48,49] and is size-consistent.

Now we proceed to show that ΔMPn takes into account linked-disconnected diagrams such as J and thus includes the corrections due to the frequency dependence of the exact self-energy. We take $n = 3$ as an example and make the following modification to the partitioning of the Hamiltonian, so that $\Sigma_x^{(1)}(\omega)$ is no longer zero and there is a nonvanishing correction due to the frequency dependence at the third order.

Assuming the canonical HF orbitals of the N-electron system, we set

$$\hat{H}_0 = E_{\mathrm{HF}} + \sum_p \epsilon_p\{\hat{p}^\dagger \hat{p}\} + \sum_p \zeta_p\{\hat{p}^\dagger \hat{p}\} \tag{38}$$

$$\hat{V} = \frac{1}{4}\sum_{p,q,r,s}\langle pq||rs\rangle\{\hat{p}^\dagger \hat{q}^\dagger \hat{s}\hat{r}\} - \sum_p \zeta_p\{\hat{p}^\dagger \hat{p}\} \tag{39}$$

where E_{HF} is the HF energy of the N-electron system in the ground state, ζ_p is a constant shift (whose value is independent of p), and $\{...\}$ denotes a normal-ordered sequence of operators.[54] They lead to

$${}^{N-1}E_x^{(0)} = E_{\mathrm{HF}} - \epsilon_x - \zeta_x \tag{40}$$

$${}^{N-1}E_x^{(1)} = \zeta_x \tag{41}$$

and

$${}^{N}E_0^{(0)} = E_{\mathrm{HF}} \tag{42}$$

$${}^{N}E_0^{(1)} = 0 \tag{43}$$

Therefore

$$\Sigma_x^{(0)}(\omega) = {}^{N}E_0^{(0)} - {}^{N-1}E_x^{(0)} = \epsilon_x + \zeta_x \tag{44}$$

$$\Sigma_x^{(1)}(\omega) = {}^{N}E_0^{(1)} - {}^{N-1}E_x^{(1)} = -\zeta_x \tag{45}$$

Note that neither is dependent on ω.

As discussed above, we expect the frequency dependence of the self-energy (such as diagram J) to be disconnected. It is also well-established that MP3 (or MPn at any order) for the N-electron system is free of disconnected (or unlinked) diagrams.[47,54] It must, therefore, come from the incomplete cancellation of disconnected terms in the $(N-1)$-electron system. In other words, we aim to show that

$$\left.\frac{\partial\Sigma_x^{(2)}(\omega)}{\partial\omega}\right|_{\epsilon_x}\Sigma_x^{(1)}(\epsilon_x) = \{{}^{N}E_0^{(3)}\}_{\mathrm{dc}} - \{{}^{N-1}E_0^{(3)}\}_{\mathrm{dc}} \tag{46}$$

with

$$\{{}^{N}E_0^{(3)}\}_{\mathrm{dc}} = 0 \tag{47}$$

$$\{{}^{N-1}E_0^{(3)}\}_{\mathrm{dc}} = -E_x^{(1)}\langle\Phi_x|\hat{V}\hat{R}\hat{R}\hat{V}|\Phi_x\rangle + \langle\Phi_x|\hat{V}\hat{R}\hat{V}\hat{R}\hat{V}|\Phi_x\rangle_{\mathrm{dc}} \tag{48}$$

where subscript dc stands for disconnected contributions and superscript $N-1$ is omitted in eq 48 and thereafter. Note that the first term in eq 48 is entirely a disconnected contribution because it is a simple product of two factors (thus carrying no dc qualifier). In the left-hand side of eq 46, we need not consider $(\partial\Sigma_x^{(1)}/\partial\omega)_{\epsilon_x}\Sigma_x^{(2)}(\epsilon_x)$ because the derivative factor is zero, as per eq 45.

The nonvanishing contributions in $\langle\Phi_x|\hat{V}\hat{R}\hat{R}\hat{V}|\Phi_x\rangle$ arise from the 2h-1p (two-hole, one-particle) and 3h-2p (three-hole, two-particle) sectors of the resolvent

$$\langle\Phi_x|\hat{V}\hat{R}\hat{R}\hat{V}|\Phi_x\rangle = \frac{1}{2}\sum_{i,j,a}\frac{\langle\Phi_x|\hat{V}|\Phi_{ij}^a\rangle\langle\Phi_{ij}^a|\hat{V}|\Phi_x\rangle}{(E_x - E_{ij}^a)^2} + \frac{1}{12}\sum_{i,j,k,a,b}\frac{\langle\Phi_x|\hat{V}|\Phi_{ijk}^{ab}\rangle\langle\Phi_{ijk}^{ab}|\hat{V}|\Phi_x\rangle}{(E_x - E_{ijk}^{ab})^2} \tag{49}$$

$$\begin{aligned}
&= \frac{1}{2}\sum_{i,j,a}\frac{\langle ij||ax\rangle\langle ax||ij\rangle}{(\epsilon_i + \epsilon_j - \epsilon_a - \epsilon_x)^2} + \frac{1}{4}\sum_{i\neq x,j\neq x,a,b}\frac{\langle ij||ab\rangle\langle ab||ij\rangle}{(\epsilon_i + \epsilon_j - \epsilon_a - \epsilon_b)^2} \\
&= \frac{1}{2}\sum_{i,j,a}\frac{\langle ij||ax\rangle\langle ax||ij\rangle}{(\epsilon_i + \epsilon_j - \epsilon_a - \epsilon_x)^2} + \frac{1}{4}\sum_{i,j,a,b}\frac{\langle ij||ab\rangle\langle ab||ij\rangle}{(\epsilon_i + \epsilon_j - \epsilon_a - \epsilon_b)^2} - \frac{1}{2}\sum_{j,a,b}\frac{\langle xj||ab\rangle\langle ab||xj\rangle}{(\epsilon_x + \epsilon_j - \epsilon_a - \epsilon_b)^2}
\end{aligned} \tag{50}$$

where $E_x = \langle\Phi_x|\hat{H}_0|\Phi_x\rangle$, $E_{ij}^a = \langle\Phi_{ij}^a|\hat{H}_0|\Phi_{ij}^a\rangle$, etc. The disconnected contribution in $\langle\Phi_x|\hat{V}\hat{R}\hat{V}\hat{R}\hat{V}|\Phi_x\rangle$ comes from the 3h-2p sector only

$$\begin{aligned}
&\langle\Phi_x|\hat{V}\hat{R}\hat{V}\hat{R}\hat{V}|\Phi_x\rangle_{\mathrm{dc}} \\
&= \frac{1}{144}\sum_{i,\ldots,d}^{\mathrm{dc}}\frac{\langle\Phi_x|\hat{V}|\Phi_{ijk}^{ab}\rangle\langle\Phi_{ijk}^{ab}|\hat{V}|\Phi_{lmn}^{cd}\rangle\langle\Phi_{lmn}^{cd}|\hat{V}|\Phi_x\rangle}{(E_x - E_{ijk}^{ab})(E_x - E_{lmn}^{cd})} \\
&= \frac{1}{4}\sum_{i\neq x,j\neq x,a,b}^{\mathrm{dc}}\frac{\langle ij||ab\rangle\langle ab||ij\rangle}{(\epsilon_i + \epsilon_j - \epsilon_a - \epsilon_b)^2}\times(\zeta_i + \zeta_j + \zeta_x - \zeta_a - \zeta_b)
\end{aligned} \tag{51}$$

$$\begin{aligned}
&= \frac{1}{4}\sum_{i,j,a,b}\frac{\langle ij||ab\rangle\langle ab||ij\rangle}{(\epsilon_i + \epsilon_j - \epsilon_a - \epsilon_b)^2}\zeta_x - \frac{1}{2}\sum_{j,a,b}\frac{\langle xj||ab\rangle\langle ab||xj\rangle}{(\epsilon_x + \epsilon_j - \epsilon_a - \epsilon_b)^2}(2\zeta_x)
\end{aligned} \tag{52}$$

In the last equality, we have used the fact that the terms in eq 51 containing factors of ζ_i, ζ_j, ζ_a, and ζ_b are connected because

DOI: 10.1021/acs.jctc.5b00005
J. Chem. Theory Comput. 2015, 11, 1595−1606

i, j, a, and b are among the summation indexes, whereas the term containing ζ_x is disconnected.

Substituting eqs 50 and 52 into eq 48, we obtain

$$E_x^{(1)}\langle\Phi_x|\hat{V}\hat{R}\hat{R}\hat{V}|\Phi_x\rangle - \langle\Phi_x|\hat{V}\hat{R}\hat{V}\hat{R}\hat{V}|\Phi_x\rangle_{\mathrm{dc}} = -\frac{1}{2}\sum_{i,j,a}\frac{\langle ij||ax\rangle\langle ax||ij\rangle}{(\epsilon_i+\epsilon_j-\epsilon_a-\epsilon_x)^2}(-\zeta_x) - \frac{1}{2}\sum_{j,a,b}\frac{\langle xj||ab\rangle\langle ab||xj\rangle}{(\epsilon_x+\epsilon_j-\epsilon_a-\epsilon_b)^2}(-\zeta_x) \quad (53)$$

which is found to be equal to the left-hand side of eq 46. Essentially the same proof can be constructed for ΔMP3 between the $(N+1)$- and N-electron systems.

We have shown that ΔMP3 (with a modified partitioning of the Hamiltonian) contains the third-order correction due to the frequency dependence of the exact self-energy in the form of eq 35. We conjecture that this holds true at higher orders and with the Møller−Plesset partitioning of the Hamiltonian, making ΔMPn converge at the exact, self-consistent solutions of the Dyson equation as $n \to \infty$.

4.3. Relationship to EOM-CC. The diagrammatic correspondence between the CC and MP methods for the ground state is well-established.[54,60] Since the IP- and EA-EOM-CC methods with the N-electron HF reference wave function yield converging results for electron binding energies, they should account for all diagrammatic contributions in ΔMPn. Here, we show that self-energy diagrams B and C (Figure 1) as well as semireducible diagrams H and I (Figure 6) and linked-disconnected diagram J (Figure 7) of ΔMPn are indeed included in IP-EOM-CCSD in the case of electron-detachment energies.

The CI-like eigenvalue equations of IP-EOM-CCSD can be written as

$$-\omega r_k = -\epsilon_k r_k - \frac{1}{2}\sum_{i,j,a}\langle ij||ak\rangle r_{ij}^a - \frac{1}{2}\sum_{i,j,a,b}\langle ij||ab\rangle t_{ik}^{ab} r_j + \ldots \quad (54)$$

$$-\omega r_{ij}^a = (-\epsilon_i - \epsilon_j + \epsilon_a) r_{ij}^a - \sum_k \langle ak||ij\rangle r_k + \ldots \quad (55)$$

where only relevant terms are shown and the eigenvalue (electron-detachment energy), ω, is multiplied by −1 to facilitate the correspondence with ΔMPn. Here, t_{ij}^{ab} is the amplitude of the cluster excitation operator, which is known from the preceding CCSD calculation, and r_k and r_{ij}^a are the amplitudes of the 1h and 2h-1p ionization operators to be determined by solving these equations.

The zeroth-order perturbation approximations to ω and r_k for the Koopmans-like final state in which the xth orbital is vacant are

$$^{(0)}\Sigma_x = \epsilon_x \quad (56)$$

$$^{(0)}r_k = \delta_{kx} \quad (57)$$

Substituting these into eq 55 truncated after the second term yields the first-order approximation to r_{ij}^a as

$$^{(1)}r_{ij}^a = \frac{\langle ax||ij\rangle}{\epsilon_x+\epsilon_a-\epsilon_i-\epsilon_j} \quad (58)$$

The corresponding approximation to t_{ij}^{ab} is the MP1 excitation amplitude

$$^{(1)}t_{ij}^{ab} = \frac{\langle ab||ij\rangle}{\epsilon_i+\epsilon_j-\epsilon_a-\epsilon_b} \quad (59)$$

Substituting these into eq 54 gives the second-order correction to ω, which reads

$$^{(2)}\Sigma_x = \frac{1}{2}\sum_{i,j,a}\langle ij||ax\rangle\,{}^{(1)}r_{ij}^a + \frac{1}{2}\sum_{i,j,a,b}\langle ij||ab\rangle\,{}^{(1)}t_{ix}^{ab}\,{}^{(0)}r_j = \frac{1}{2}\sum_{i,j,a}\frac{\langle ij||ax\rangle\langle ax||ij\rangle}{\epsilon_x+\epsilon_a-\epsilon_i-\epsilon_j} + \frac{1}{2}\sum_{i,a,b}\frac{\langle ab||ix\rangle\langle ix||ab\rangle}{\epsilon_x+\epsilon_i-\epsilon_a-\epsilon_b} \quad (60)$$

which agrees exactly with the sum of eqs 13 and 14 at $\omega = \epsilon_x$ (diagrams B and C). Here, we define the perturbation order by the number of appearances of the fluctuation potential in each term.

A part of the second-order correction to r_k can be obtained by substituting eqs 56−58 into eq 54 truncated after the second term, yielding

$$^{(2)}r_{k\neq x} = \{^{(0)}\Sigma_x - \epsilon_k\}^{-1}\frac{1}{2}\sum_{i,j,a}\langle ij||ak\rangle\,{}^{(1)}r_{ij}^a = \frac{1}{2}\sum_{i,j,a}\frac{\langle ax||ij\rangle\langle ij||ak\rangle}{(\epsilon_x+\epsilon_a-\epsilon_i-\epsilon_j)(\epsilon_x-\epsilon_k)} \quad (61)$$

Note that this expression is valid only for $k \neq x$, lest it diverges. This in conjunction with eq 55 truncated after the second term suggests the third-order correction to r_{ij}^a as

$$^{(3a)}r_{ij}^a = \{^{(0)}\Sigma_x + \epsilon_a - \epsilon_i - \epsilon_j\}^{-1}\sum_k\langle ak||ij\rangle\,{}^{(2)}r_{k\neq x} = \frac{1}{2}\sum_{l,m,b}\sum_{k\neq x}\frac{\langle bx||lm\rangle\langle lm||bk\rangle\langle ak||ij\rangle}{(\epsilon_x+\epsilon_b-\epsilon_l-\epsilon_m)(\epsilon_x-\epsilon_k)(\epsilon_x+\epsilon_a-\epsilon_i-\epsilon_j)} \quad (62)$$

Its substitution into the second term in the right-hand side of eq 54 leads to a fourth-order correction to ω

$$^{(4a)}\Sigma_x = \frac{1}{2}\sum_{i,j,a}\langle ij||ax\rangle\,{}^{(3a)}r_{ij}^a = \frac{1}{4}\sum_{i,j,a}\sum_{l,m,b}\sum_{k\neq x}\frac{\langle bx||lm\rangle\langle lm||bk\rangle\langle ak||ij\rangle\langle ij||ax\rangle}{(\epsilon_x+\epsilon_b-\epsilon_l-\epsilon_m)(\epsilon_x-\epsilon_k)(\epsilon_x+\epsilon_a-\epsilon_i-\epsilon_j)} \quad (63)$$

which is exactly the contribution from semireducible diagram H at $\omega = \epsilon_x$, accounting for the off-diagonal elements of the irreducible self-energy (diagram C). The index restriction, $k \neq x$, distinguishes this term from reducible diagram E.

Another third-order correction to r_{ij}^a can be obtained by adopting the second-order approximation for ω in eq 55 truncated after the second term

$$^{(1)}r_{ij}^a + {}^{(3b)}r_{ij}^a = \{^{(2)}\Sigma_x + {}^{(0)}\Sigma_x + \epsilon_a - \epsilon_i - \epsilon_j\}^{-1}\sum_k\langle ak||ij\rangle\,{}^{(0)}r_k \approx \frac{\langle ax||ij\rangle}{\epsilon_x+\epsilon_a-\epsilon_i-\epsilon_j} - \frac{{}^{(2)}\Sigma_x\langle ax||ij\rangle}{(\epsilon_x+\epsilon_a-\epsilon_i-\epsilon_j)^2} \quad (64)$$

In the second equality, a use is made of the Maclaurin series: $(1+\delta)^{-1} \approx 1-\delta$, with $\delta = {}^{(2)}\Sigma_x/(\epsilon_x+\epsilon_a-\epsilon_i-\epsilon_j)$. Substitution of the third-order correction into eq 54 gives a fourth-order correction to ω in the form

DOI: 10.1021/acs.jctc.5b00005
J. Chem. Theory Comput. 2015, 11, 1595−1606

$$
\begin{aligned}
{}^{(4b)}\Sigma_x &= \frac{1}{2}\sum_{i,j,a}\langle ij||ax\rangle\ {}^{(3b)}r_{ij}^{a} \\
&= -\frac{1}{2}\sum_{i,j,a}\frac{\langle ax||ij\rangle\langle ij||ax\rangle}{\left(\epsilon_x+\epsilon_a-\epsilon_i-\epsilon_j\right)^2}\,{}^{(2)}\Sigma_x
\end{aligned}
\tag{65}
$$

which accounts for two of the linked-disconnected diagram contributions in the last term of eq 36 analogous to diagram J.

Nooijen and Snijders pointed out[61,62] that IP- and EA-EOM-CC can be viewed as a GF theory.

5. CONCLUSIONS

An nth-order self-energy can be defined as the difference in MPn energy between the N- and $(N \pm 1)$-electron systems (ΔMPn), which are, in turn, evaluated by the determinant-based, general-order MPn method[1] at any n. This constitutes a general-order implementation of a one-electron GF method.

The electron binding energies calculated with ΔMPn ($n \leq 3$) agree identically with the solutions of the Dyson equation in the diagonal and frequency-independent approximations to the self-energy. However, the converged limits of the binding energies at $n = \infty$ (if they do converge) are the exact basis-set values, that is, the solutions of the Dyson equation with the exact, nondiagonal, frequency-dependent self-energy. This suggests that the electron binding energies of ΔMPn include perturbation corrections due to the off-diagonal elements and frequency dependence of the self-energy, which may be zero at $n \leq 3$ but are nonzero elsewhere. Therefore, ΔMPn defines a new, converging expansion of the exact self-energies for Koopmans-like transitions, whose computer implementation does not involve diagonalization or self-consistent solutions of a recursive equation. Our diagrammatic analysis shows that these corrections are accounted for by semireducible and linked-disconnected diagrams. The lowest order at which these diagrams appear is four and these fourth-order diagrams are also included in IP- or EA-EOM-CCSD.

In CH^+, the electron binding energies of ΔMPn display smooth, nearly monotonic convergence at $n > 2$, unless they display a sign of divergence. Padé approximants are shown to extrapolate the correct limit within a few mE_h from these apparently divergent series. In C_2, the electron binding energies of the four frontier orbitals are oscillatory but convergent. The approximations defined by ΔMPn are, therefore, expected to be useful up to high orders and especially so when combined with Padé approximants in the case of divergent series. Each diagrammatic contribution of ΔMPn can be recast into a single high-dimensional integral and subject to a highly scalable Monte Carlo evaluation,[63] owing to the aforementioned inherent algorithmic simplicity.

AUTHOR INFORMATION

Corresponding Author

*E-mail: sohirata@illinois.edu.

Funding

This work was supported by the SciDAC program of the U.S. Department of Energy, Office of Science, Basic Energy Sciences, under award no. DE-FG02-12ER46875 and CREST, Japan Science and Technology Agency.

Notes

The authors declare no competing financial interest.

ACKNOWLEDGMENTS

S.H. is a Camille Dreyfus Teacher-Scholar and a Scialog Fellow of the Research Corporation for Science Advancement.

REFERENCES

(1) Knowles, P. J.; Somasundram, K.; Handy, N. C.; Hirao, K. *Chem. Phys. Lett.* **1985**, *113*, 8−12.
(2) Knowles, P. J.; Handy, N. C. *Chem. Phys. Lett.* **1984**, *111*, 315−321.
(3) Hirata, S.; Bartlett, R. J. *Chem. Phys. Lett.* **2000**, *321*, 216−224.
(4) Kállay, M.; Surján, P. R. *J. Chem. Phys.* **2000**, *113*, 1359−1365.
(5) Olsen, J. *J. Chem. Phys.* **2000**, *113*, 7140−7148.
(6) Hirata, S.; Nooijen, M.; Bartlett, R. J. *Chem. Phys. Lett.* **2000**, *326*, 255−262.
(7) Hirata, S.; Nooijen, M.; Bartlett, R. J. *Chem. Phys. Lett.* **2000**, *328*, 459−468.
(8) Stanton, J. F.; Bartlett, R. J. *J. Chem. Phys.* **1993**, *98*, 7029−7039.
(9) Nooijen, M.; Bartlett, R. J. *J. Chem. Phys.* **1995**, *102*, 3629−3647.
(10) Linderberg, J.; Öhrn, Y. *Propagators in Quantum Chemistry*; Academic Press: London, 1973.
(11) Cederbaum, L. S.; Domcke, W. *Adv. Chem. Phys.* **1977**, *36*, 205−344.
(12) Simons, J. *Annu. Rev. Phys. Chem.* **1977**, *28*, 15−45.
(13) Jørgensen, P.; Simons, J. *Second Quantization-Based Methods in Quantum Chemistry*; Academic Press: New York, 1981.
(14) Öhrn, Y.; Born, G. *Adv. Quantum Chem.* **1981**, *13*, 1−88.
(15) Herman, M. F.; Freed, K. F.; Yeager, D. L. *Adv. Chem. Phys.* **1981**, *48*, 1−69.
(16) von Niessen, W.; Schirmer, J.; Cederbaum, L. S. *Comput. Phys. Rep.* **1984**, *1*, 57−125.
(17) Oddershede, J. *Adv. Chem. Phys.* **1987**, *69*, 201−239.
(18) Ortiz, J. V. *Adv. Quantum Chem.* **1999**, *35*, 33−52.
(19) Danovich, D. *Wiley Interdiscip. Rev.: Comput. Mol. Sci.* **2011**, *1*, 377−387.
(20) Suhai, S. *Phys. Rev. B* **1983**, *27*, 3506−3518.
(21) Sun, J.-Q.; Bartlett, R. J. *Phys. Rev. Lett.* **1996**, *77*, 3669−3672.
(22) Hirata, S.; Shimazaki, T. *Phys. Rev. B* **2009**, *80*, 085118.
(23) Willow, S. Y.; Kim, K. S.; Hirata, S. *Phys. Rev. B* **2014**, *90*, 201110(R).
(24) Onida, G.; Reining, L.; Rubio, A. *Rev. Mod. Phys.* **2002**, *74*, 601−659.
(25) Pickup, B. T.; Goscinski, O. *Mol. Phys.* **1973**, *26*, 1013−1035.
(26) Mattuck, R. D. *A Guide to Feynman Diagrams in the Many-Body Problem*; Dover: New York, 1992.
(27) March, N. H.; Young, W. H.; Sampanthar, S. *The Many-Body Problem in Quantum Mechanics*; Cambridge University Press: Cambridge, 1967.
(28) Cederbaum, L. S.; Hohlneicher, G.; Niessen, W. *Chem. Phys. Lett.* **1973**, *18*, 503−508.
(29) Simons, J.; Smith, W. D. *J. Chem. Phys.* **1973**, *58*, 4899−4907.
(30) Redmon, L. T.; Purvis, G.; Öhrn, Y. *J. Chem. Phys.* **1975**, *63*, 5011−5017.
(31) Purvis, G. D.; Öhrn, Y. *Chem. Phys. Lett.* **1975**, *33*, 396−398.
(32) Jørgensen, P.; Simons, J. *J. Chem. Phys.* **1975**, *63*, 5302−5304.
(33) Herman, M. F.; Yeager, D. L.; Freed, K. F. *Chem. Phys.* **1978**, *29*, 77−96.
(34) Zakrzewski, V. G.; Ortiz, J. V. *Int. J. Quantum Chem.* **1995**, *53*, 583−590.
(35) Ortiz, J. V. *J. Chem. Phys.* **1996**, *104*, 7599−7605.
(36) Ortiz, J. V.; Zakrzewski, V. G. *J. Chem. Phys.* **1996**, *105*, 2762−2769.
(37) Ortiz, J. V. *Int. J. Quantum Chem.* **1997**, *63*, 291−299.
(38) Ortiz, J. V. *J. Chem. Phys.* **1998**, *108*, 1008−1014.
(39) Ferreira, A. M.; Seabra, G.; Dolgounitcheva, O.; Zakrzewski, V. G.; Ortiz, J. V. In *Quantum-Mechanical Prediction of Thermochemical Data*; Cioslowski, J., Ed.; Kluwer Academic Publishers: Boston, MA, 2001; pp 131−160.
(40) Schirmer, J.; Cederbaum, L. S.; Walter, O. *Phys. Rev. A* **1983**, *28*, 1237−1259.

DOI: 10.1021/acs.jctc.5b00005
J. Chem. Theory Comput. 2015, 11, 1595−1606

(41) Ortiz, J. V. *J. Chem. Phys.* **1988**, *89*, 6348−6352.
(42) Ortiz, J. V. *J. Chem. Phys.* **1988**, *89*, 6353−6356.
(43) Nobes, R. H.; Pople, J. A.; Radom, L.; Handy, N. C.; Knowles, P. J. *Chem. Phys. Lett.* **1987**, *138*, 481−485.
(44) Chong, D. P.; Herring, F. G.; McWilliams, D. *J. Chem. Phys.* **1974**, *61*, 78−84.
(45) Chong, D. P.; Herring, F. G.; McWilliams, D. *J. Chem. Phys.* **1974**, *61*, 958−962.
(46) Chong, D. P.; Herring, F. G.; McWilliams, D. *J. Chem. Phys.* **1974**, *61*, 3567−3570.
(47) Szabo, A.; Ostlund, N. S. *Modern Quantum Chemistry*; MacMillan: New York, 1982.
(48) Hirata, S. *Theor. Chem. Acc.* **2011**, *129*, 727−746.
(49) Hirata, S.; Keçeli, M.; Ohnishi, Y.; Sode, O.; Yagi, K. *Annu. Rev. Phys. Chem.* **2012**, *63*, 131−153.
(50) Hermes, M. R.; Hirata, S. *J. Chem. Phys.* **2013**, *139*, 034111.
(51) Bloch, C.; De Dominicis, C. *Nucl. Phys.* **1958**, *7*, 459−479.
(52) Bloch, C. In *Studies in Statistical Mechanics*; De Boer, J., Uhlenbeck, G. E., Eds.; North-Holland: Amsterdam, 1965; pp 3−211.
(53) Hirata, S.; He, X.; Hermes, M. R.; Willow, S. Y. *J. Phys. Chem. A* **2014**, *118*, 655−672.
(54) Shavitt, I., Bartlett, R. J. *Many-Body Methods in Chemistry and Physics*; Cambridge University Press: Cambridge, 2009.
(55) Olsen, J.; Christiansen, O.; Koch, H.; Jørgensen, P. *J. Chem. Phys.* **1996**, *105*, 5082−5090.
(56) Sergeev, A. V.; Goodson, D. Z.; Wheeler, S. E.; Allen, W. D. *J. Chem. Phys.* **2005**, *123*, 064105.
(57) Laidig, W. D.; Fitzgerald, G.; Bartlett, R. J. *Chem. Phys. Lett.* **1985**, *113*, 151−158.
(58) Kamiya, M.; Hirata, S. *J. Chem. Phys.* **2006**, *125*, 074111.
(59) Kamiya, M.; Hirata, S. *J. Chem. Phys.* **2007**, *126*, 134112.
(60) Bartlett, R. J. *Annu. Rev. Phys. Chem.* **1981**, *32*, 359−401.
(61) Nooijen, M.; Snijders, J. G. *Int. J. Quantum Chem.* **1992**, *S26*, 55−83.
(62) Nooijen, M.; Snijders, J. G. *Int. J. Quantum Chem.* **1993**, *48*, 15−48.
(63) Willow, S. Y.; Kim, K. S.; Hirata, S. *J. Chem. Phys.* **2013**, *138*, 164111.

DOI: 10.1021/acs.jctc.5b00005
J. Chem. Theory Comput. 2015, 11, 1595−1606